Limnol. Oceanogr., 51(1), 2006, 142–156

Bioirrigation in permeable sediments: Advective pore-water transport induced by burrow ventilation

Filip J. R. Meysman,[1] *Oleksiy S. Galaktionov, Britta Gribsholt, and Jack J. Middelburg*
The Netherlands Institute of Ecology (NIOO-KNAW), Centre for Estuarine and Marine Ecology, Korringaweg 7, 4401 NT Yerseke, The Netherlands

Abstract

The physical mechanism that drives bioirrigation is strongly dependent on the permeability of the sediment. We advance two mechanisms, each described by a corresponding microenvironment model. In muds, burrow water cannot penetrate the sediment, so bioirrigation is intrinsically driven by diffusional transfer across the burrow wall. This ''diffusive'' mode of bioirrigation is accurately described by the classical tube irrigation model. In sands, ventilation flows can penetrate the surrounding sediment via dead end burrows. To quantify this ''advective'' mode of bioirrigation, we propose a novel two-dimensional pocket injection model. This model's principal features are that (1) organisms indent the sediment–water interface with burrow structures, (2) the specific structure of the burrow can be neglected except for the location of a feeding pocket, and (3) burrow water is injected from this feeding pocket into the surrounding sediment. We tested the adequacy of the pocket injection model in a detailed case study of the lugworm *Arenicola marina,* comparing model simulations and experimental data from core incubations. Simulation of two different sets of inert tracer experiments shows good agreement between model and data, indicating that our model captures the relevant aspects of lugworm bioirrigation in permeable sediments.

Diverse macrobenthic communities inhabit the surface layer of marine and estuarine sediments, supported by fluxes of organic matter and oxygen across the sediment–water interface. A major fraction of these bottom dwellers create burrows or burrow networks that penetrate deeply into the anoxic zone of the sediment (Anderson and Meadows 1978). The metabolic demand for oxygen is satisfied through passive or active flushing of the burrows with oxygen-rich water from the overlying water column (Gust and Harrison 1981; Webb and Eyre 2004). Besides oxygen supply, burrow flushing has also been linked to metabolite removal and filter feeding (Aller 2001). This process of burrow flushing and its geochemical consequences is typically referred to as *bioirrigation* (Rhoads 1974; Aller 2001). Previous studies have shown that bioirrigation exerts a major control on sediment biogeochemistry (Davis 1974; Aller and Aller 1998; Wenzhöfer and Glud 2004), microbial ecology (Hylleberg 1975; Reichardt 1988; Marinelli et al. 2002), and solute exchange across the sediment–water interface (Christensen et al. 1984; Archer and Devol 1992; Meile and Van Cappellen 2003). Therefore, the development of reactive transport models for aquatic sediments crucially depends on a—preferably mechanistic—mathematical description of bioirrigation.

In the past, a suite of bioirrigation models have been proposed that can be classified into two general approaches (Aller 2001). A first category of models can be qualified tentatively as ''phenomenological'' because the principal aim is to accurately reproduce depth profiles of solute concentrations, reaction rates in sediments, or both. Accordingly, these models pragmatically focus on the consequence—the enhanced pore-water transport and its influence on diagenetic processes—rather than the cause—the underlying burrow-flushing activity that drives the pore-water transport. Typically, such phenomenological models involve a modification of either the diffusive (e.g., Vanderborght et al. 1977; Berner 1980; Berg et al. 2001), the advective (e.g., Hammond et al. 1975; Benoit et al. 1991), or the source/sink term (e.g., McCaffrey et al. 1980; Emerson et al. 1984; Meile et al. 2001) in the one-dimensional early diagenetic equation. A second category of bioirrigation models could be termed ''mechanistic'' in the sense that (1) they explicitly link burrow flushing (the cause) to solute transport in the pore water (the consequence), and (2) they explicitly account for the three-dimensional nature of bioirrigation, rather than emulating the effect on solute transport in a one-dimensional fashion.

To date, all bioirrigation models within the mechanistic category essentially trace back to the tube irrigation model of Aller (1980), which can be regarded as a true milestone in the quantitative approach to bioirrigation. In this tube irrigation model, the sediment is idealized as a collection of identical adjacent ''microenvironments'' or ''territories,'' each inhabited by a single burrowing organism (Fig. 1a). The model's original formulation was based on the following assumptions (Aller 1980): (1) a microenvironment is a cylindrical domain with a cylindrical void space in the center representing the burrow, (2) burrows have an identical geometry and are equidistantly spaced, (3) the organism vigorously mixes the burrow water so that its composition always equals that of the overlying water, and (4) the actual process of bioirrigation is caused by radial diffusion of solutes from the burrow water, through the burrow wall into

[1] Corresponding author (f.meysman@nioo.knaw.nl).

Acknowledgments

The instructive comments of Bob Aller and an anonymous reviewer significantly improved the manuscript.

This research was supported by grants from the European Union (project NAME, EVK 3-CT-2001-00066; project COSA, EVK 3-CT-2002-00076) and by a PIONIER grant from the Netherlands Organization for Scientific Research (NWO, 833.02.2002).

This is publication 3573 of the NIOO-KNAW (Netherlands Institute of Ecology).

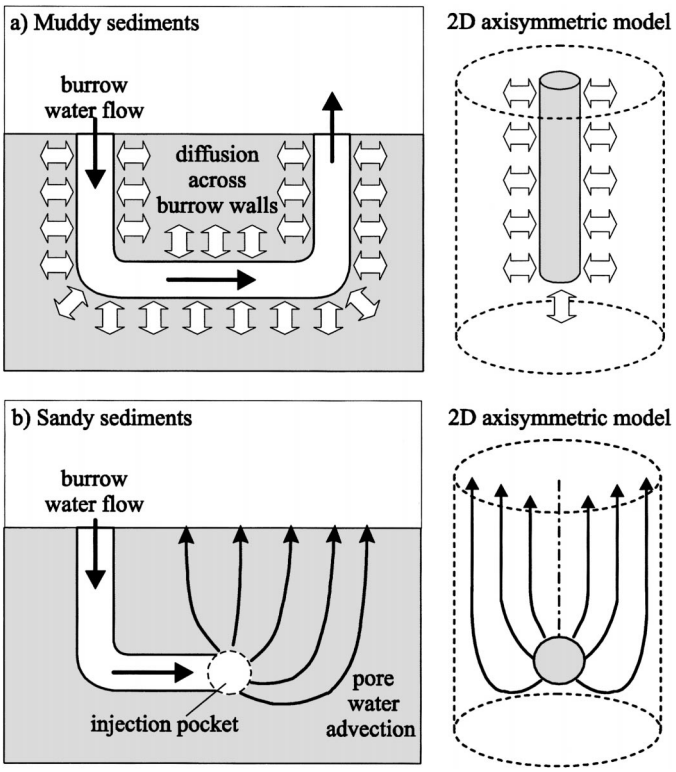

Fig. 1. Conceptual bioirrigation scheme and corresponding microenvironment model for two end-members of sediment permeability. (a) Muddy environments. Diffusive transfer across the walls of U-shaped burrow. Idealized model geometry of the corresponding 2D tube irrigation model by Aller (1980). (b) Sandy environments. Advective injection at the end of a J-shaped burrow. Idealized model geometry of the corresponding 2D pocket injection model.

the surrounding sediment. Subsequent studies relaxed some of the assumptions in the original Aller (1980) formulation. Boudreau and Marinelli (1994) investigated the effects of periodic, discontinuous ventilation of burrows, resulting in a nonhomogeneous burrow water composition. Furukawa et al. (2001) extended the model to burrows that have a depth-dependent radius and tilt angle. Koretsky et al. (2002) applied the model to stochastic realizations of burrow networks. Nonetheless, these model extensions retained the fundamental principle underlying the Aller (1980) model: bioirrigational transport is in essence a diffusive transfer mechanism.

This ''diffusive'' link between burrow flushing and porewater transport seems appropriate in muddy environments but does not apply to the bioirrigation activity of some dominant macrofauna in sandy sediments. Because of higher permeability, advective transport dominates diffusive transport in sandy environments (Huettel and Webster 2001). Therefore, when ventilating their burrows, organisms are able to actively pump water across the burrow wall, and these advective flows will penetrate the sediment surrounding the burrow (Foster-Smith 1978; Huettel 1990). The resulting upward percolation of injected burrow water forces pore water out of the sediment (Fig. 1b), and this advective mechanism

Table 1. Compilation of parameters for a ''standard'' lugworm and dimensions for a typical microenvironment. The subscripts ''b'' and ''t'' refer to burrow and territory, respectively, whereas SEF is the surface enlargement factor.

Parameter	Value	Units
Individual		
Wet weight (W_w)	3.5*	g
Pumping rate (Q)	1.50*†	$cm^3\ min^{-1}$
Burrow		
Radius (R_b)	0.25*	cm
Length (L_b)	25	cm
Surface area ($A_b = 2\pi R_b L_b$)	39	cm^2
Volume ($V_b = \pi R_b^2 L_b$)	4.9	cm^3
Territory		
Density (n)	25‡	$ind\ m^{-2}$
Cross-sectional area ($A_t = n^{-1}$)	400	cm^2
Depth (L_t)	20	cm
Volume ($V_t = A_t L_t$)	8,000	cm^3
SEF (A_b/A_t)	0.1	

* Riisgård et al. 1996.
† Kristensen et al. 2001.
‡ Riisgård and Banta 1998.

of solute transfer has been hypothesized to be more efficient than the radial diffusion of solutes from the burrow water into the surrounding pore water (Riisgård and Banta 1998; Kristensen 2001). The aim of this work is to present a conceptual microenvironment model for advective solute transport in sandy sediments induced by the flushing of macrofaunal burrows. This model is termed the two-dimensional (2D) pocket injection model, and effectively, it can be regarded as the advective counterpart of Aller's ''diffusive'' 2D tube irrigation model. The adequacy of the model is tested in a case study of bioirrigation induced by the lugworm *Arenicola marina*, which is a dominant bioirrigator of sandy coastal and estuarine sediments across Europe (Huettel 1990; Riisgård and Banta 1998). The 2D pocket injection model generates velocity fields and concentration patterns in the sediment environment surrounding the lugworm's burrow. To assess the predictive capabilities of the model, these simulation results are compared with published data and results from new experiments with inert tracers.

Materials and methods

Modeling approach—Details on the feeding, burrowing, respiration, and ventilation activity of *A. marina* can be found in reviews (Kruger 1971; Riisgård and Banta 1998; Kristensen 2001). Here, we will only summarize those aspects that relate to burrow ventilation. Table 1 summarizes the parameters for a ''standard'' *A. marina* and a typical lugworm habitat that are further employed in calculation and discussion. The lugworm dwells in J-shaped burrows, and generates a water flow that is opposite the direction of the sediment transport (Fig. 1b). When pumping, the worm resides in the lower part of the burrow called the ''gallery.'' The lugworm pumps water by means of pistonlike waves that run along its dorsal surface. The suction created by these

peristaltic motions takes in oxygenated water from the overlying water column. Passing through the burrow and over the lugworm's gills, this water is subsequently pumped through the porous walls of the feeding pocket into the surrounding sediment. This creates an advective transport of pore water back to the sediment surface.

One way to investigate the temporal and spatial aspects of this advective bioirrigation is to incubate lugworms in laboratory sediment cores and perform conservative tracer experiments. To quantitatively interpret the data resulting from such core incubations, one actually needs to combine three separate models. First, one needs to develop a flow model, which simulates the pore-water velocity pattern induced by the lugworm's pumping. Subsequently, the calculated velocity should be incorporated into a reactive transport model (i.e., the mass conservation equation for the conservative tracer in the pore water). Third, one needs a so-called water column model to account for the exchange between pore water and overlying water. This mass balance model describes the tracer's concentration in the overlying water of the incubation chamber.

Model assumptions—The lugworm's bioirrigation activity takes place in a complex three-dimensional context. To manage this complexity, bioirrigation models should adopt a suitable abstraction of reality. Here, we propose a strong idealization of *A. marina*'s bioirrigation mechanism on the basis of the following three assumptions: (1) the lugworm continuously pumps burrow water at a steady pumping rate, (2) the sediment surrounding the burrow has homogeneous properties, and (3) the injection of burrow water into the sediment can be modeled as a local spherical source. Obviously, these three strong assumptions warrant appropriate discussion and justification.

The first assumption of continuous pumping seems acceptable because the lugworm's pumping activity proceeds in very regular cycles of 40 min that are probably under the control of a pacemaker in the nervous system (Wells 1949; Kruger 1971). The typical pattern shows large periods of quite steady pumping, interrupted by short periods of inactivity related to defecation at the surface (Baumfalk 1979). This contrasts strongly with the irregular ventilation pattern of other tube-dwelling organisms such as Nereid polychaetes (Kristensen 2001). Effectively, the regular and steady pattern allows an adequate characterization of the lugworm's ventilation activity in terms of a mechanical pump that operates continuously (Foster-Smith 1978; Riisgård et al. 1996; Meysman et al. in press).

The second assumption of homogeneity implies that the sediment has uniform properties (porosity, permeability, etc.) within a given lugworm ''territory.'' Under natural conditions, it has been observed that sediment reworking by benthic organisms can lead to a strong spatial variation in sediment properties (Jones and Jago 1993). In the case of *A. marina,* a coarse sediment layer is often observed at the level of the gallery and the feeding pocket, attributed to selective particle ingestion (Reise 2002). The lugworm ingests only the smaller particles; hence, the coarser material accumulates. Equally, the zone beyond the feeding funnel, where sediment slopes downward to the feeding pocket, is considered to have distinct properties (Riisgård and Banta 1998). Although prevailing in natural systems, such spatial heterogeneity requires time to develop and results from the cumulative effect of prolonged biological activity. The laboratory incubations that are considered here all start from an initially homogeneous sediment, involve only short acclimatization periods, and have limited incubation periods (1 h to 1 d). We assume that this time span is too short to develop significant heterogeneity, so we suppose that uniform sediment properties are justified when modeling the incubation experiments. However, even for natural systems, homogeneity might serve as a useful first-order assumption. The gradients in sediment properties associated with the feeding funnel and the permeable shell layer are very localized. This requires porosity and permeability measurements on a millimeter-scale resolution. Such data are not presently available, although methods are currently being developed (Rocha et al. 2005). In the absence of such data, the assumption of homogeneity emerges as the most parsimonious starting point for model development.

The third and most radical assumption in our model is that the geometry of the burrow is irrelevant, except for the shape and location of the feeding pocket, which serves as the injection pocket of burrow water into the sediment. This omission of the burrow details implies that (1) diffusion across burrow walls can be neglected compared with the advective effect of burrow water injection, and (2) the geometry of the burrow has negligible influence on the flow pattern in the pore water. The first supposition is readily illustrated in Table 2, in which we compare the ratio of the advective versus diffusive transfer in a typical lugworm burrow for the inert tracer Br^-. To this end, we assumed that the Br^- concentration remains unchanged in the burrow wa-

Table 2. Comparison of the diffusive transfer across the burrow wall and advective transfer in the feeding pocket. These transfers are calculated for the time-dependent intrusion of Br^- in a standard lugworm burrow. Two different intrusion periods are compared, corresponding to the duration of two incubation experiments discussed in the text. The molecular diffusion coefficient $D_{Br^-}^{mol} = 1.07 \times 10^{-5}$ $cm^2\ s^{-1}$ was calculated at 15°C with the relationship in Boudreau (1997) and corrected for tortuosity with the Modified Weissman relation $\theta^2 = 1 - 2\ln(\phi)$ from Boudreau (1996) to obtain the effective diffusion coefficient $D_{Br^-}^{s} = (\phi/\theta^2)D_{Br^-}^{mol} = 5.0 \times 10^{-6}$ $cm^2\ s^{-1}$. A porosity $\phi = 0.6$ is used in these calculations. The total amount of diffusing substance M_t per unit area of burrow is calculated with the formula for a semi-infinite plane (i.e., $M_t = 2C_{Br^-}^{b}\sqrt{D_{Br^-}^{s} t/\pi}$), as given in Crank (1975). The bromide concentration within the burrow is arbitrarily fixed at 1 μmol cm^{-3}, but vanishes when calculating the ratio of the two transfers. The values for the pumping rate Q and the burrow surface area A_b are taken from Table 1.

Bioirrigation mechanism		Units	Intrusion 1 h	Intrusion 1 d
Advective transfer	$T^{adv}(t) = Q_{ind}C_{Br^-}^{b}t$	μmol	90	2,160
Diffusive transfer	$T^{dif}(t) = A_b 2C_{Br^-}^{b}\sqrt{D_{Br^-}^{s} t/\pi}$	μmol	6	29
Transfer ratio	$T^{adv}(t)/T^{dif}(t)$		15	74

ter. For timescales of 1 h (as described in the ''Br^- injection experiment'' section) and 1 d (as described in the ''NO_3^- flushing experiment'' section), the advective transfer through the feeding pocket is 15 and 74 times larger, respectively, than the diffusive transfer across the burrow walls. This justifies the neglect of diffusion across burrow walls when modeling core incubations with conservative tracers.

However, the justification that the geometry of the burrow has negligible influence on the flow pattern requires more consideration. Effectively, this issue was addressed in a detailed fashion in Meysman et al. (in press), in which a comprehensive three-dimensional (3D) flow model was presented, that incorporated an explicit description of the J-shaped burrow architecture and simulated the pore-water flow in the surrounding sediment. These model simulations show that the actual boundary condition at the burrow walls has an important influence on the resulting flow pattern. Comparing model simulations in which burrow walls are either closed or open to flow, the efficiency of the lugworm oxygen intake differs by about 40%. Closed burrow walls prevent both the outflow of oxic burrow water and the inflow of anoxic pore water. Consequently, from an ecological perspective, it is highly advantageous for the lugworm to increase the flow resistance in the burrow walls. This insulation can be done either chemically or mechanically (Meysman et al. in press), the actual mechanism being irrelevant to the discussion here. The important point is that when burrow walls are made impermeable to flow, the burrow is no longer a sink for flow lines, so all flow lines end up at the sediment–water interface. With respect to flow, the burrow functions as an impenetrable object in the sediment. Within a given lugworm territory (Table 1), the volume of the burrow ($\sim$5 cm^3) is only 0.1% of the volume of the surrounding sediment ($\sim$8,000 cm^3). Therefore, we can assume that the burrow has negligible influence on the flow pattern.

Model domain—Implementation of the above assumptions leads to the pocket injection model of lugworm bioirrigation (Fig. 2a). The model domain comprises a cylindrical volume of sediment of radius R_c, partly consisting of sediment (height H_s) and partly covered by overlying water (height H_w). The overlying water column is considered a perfectly stirred volume; hence, it has uniform properties. Conversely, sediment properties are described in a spatially explicit way. Physically, the model domain represents a 3D sediment zone, yet mathematically, the model is classified as a 2D model because, with axial symmetry, it only incorporates two spatial variables (i.e., depth z into the sediment and distance r from the central symmetry axis). This cylindrical microenvironment represents either a typical lugworm territory under natural conditions or the typical container in which laboratory irrigation experiments are carried out. Because each domain contains a single organism, the density (n, organisms/cm^2) that corresponds to a given domain can be estimated as $n = (1/\pi)(R_c)^{-2}$. Inversely, given a typical density, this relation can be used to calculate the corresponding R_c value. The feeding pocket is the actual location where burrow water is injected into the sediment and is represented as a spherical void of radius R_{fp}. In the absence of any data, the radius of the feeding pocket is taken to be equal to the burrow radius (i.e., $R_{fp} = R_b$). The center of the feeding pocket is located at depth H_{fp} from the sediment–water interface along the symmetry axis of the cylindrical domain. In a first-order approach, the sediment–water interface is considered a flat surface, thus neglecting the microtopography created by the feeding pit and the defecation mound.

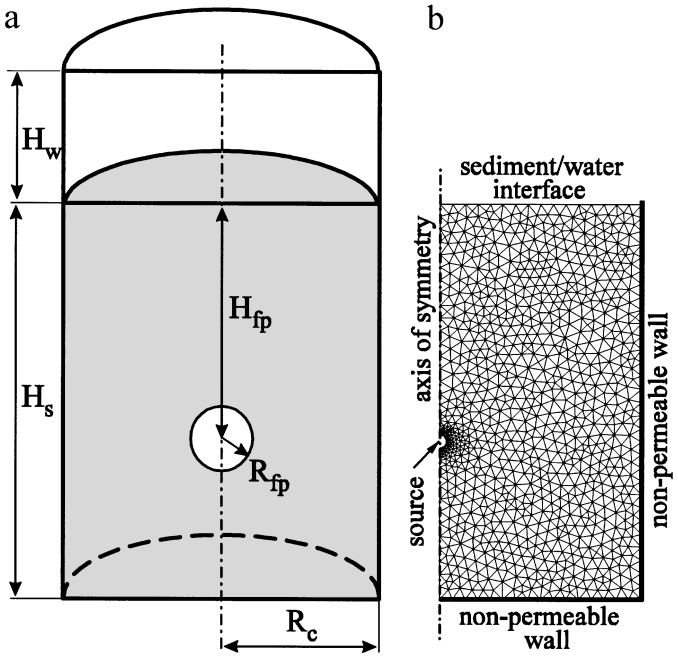

Fig. 2. (a) Microenvironment corresponding to the 2D pocket injection model of advective bioirrigation. The model domain is an axial symmetric cylinder of radius R_c consisting of an overlying water column of height H_w and a sediment column of height H_s. The feeding pocket is the only geometric feature of the lugworm burrow that is retained in the model formulation. It is modeled as a spherical source of burrow water with radius R_{fp} and located at depth H_{fp}. (b) Finite element grid for sediment part of the domain used in simulations. Because of axial symmetry, only half of the domain's cross section needs to be meshed.

Flow model (momentum conservation)—The pressure distribution and pore-water velocity field within the sediment are obtained from the conventional equations that govern transport in porous media (Bear 1972; Freeze and Cherry 1979; Bear and Bachmat 1991). The continuity equation for the incompressible pore water is given by

$$\nabla \cdot \mathbf{v}_d = 0$$

where ∇ is the gradient operator. The vector $\mathbf{v}_d$ denotes the Darcy velocity, which is related to the actual pore-water velocity $\mathbf{v}$ by $\mathbf{v}_d = \phi\mathbf{v}$, with ϕ the porosity. The resistance to flow in the sediment is described by Darcy's Law, which can be stated in the generalized form (Freeze and Cherry 1979; Bear and Bachmat 1991)

$$\mathbf{v}_d = -\frac{k}{\eta}(\nabla p - \rho g \nabla z) \tag{2}$$

where k denotes the permeability of the sediment, η the viscosity of the pore water, ρ the density of the pore water, g

is the gravitational constant, p the pressure, and z the depth coordinate measured downward from the sediment–water interface (SWI). We now introduce the excess pressure $p_e \equiv p - (p_{SWI} + \rho g z)$ as the pressure in excess over the hydrostatic pressure. Neglecting any surface topography, we assume that the pressure remains constant along the SWI (i.e., $\nabla p_{SWI} = 0$). Furthermore, we assume that the pore water is incompressible and shows no salinity gradients, resulting in a uniform density (i.e., $\nabla \rho = 0$). Under these conditions, we can substitute Darcy's Law into continuity Eq. 1 to obtain Eq. 3.

$$\nabla \cdot \left(-\frac{k}{\eta} \nabla p_e \right) = 0 \tag{3}$$

The assumption of homogeneity further implies that the permeability of the sediment and the viscosity of the pore water remain constant. Accordingly, Eq. 3 reduces to the classical Laplace equation in Eq. 4.

$$\nabla^2 p_e = 0 \tag{4}$$

Solution of Laplace Eq. 4 provides the excess pressure distribution inside the sediment domain. From this, one can subsequently calculate the associated velocity vector field by means of Eq. 2.

The solution of Laplace Eq. 4 requires appropriate boundary conditions both externally (i.e., along the outer boundaries of the sediment domain) and internally (i.e., along the feeding pocket). The formulation of the external boundary conditions is rather straightforward. At the sediment–water interface, we assume that the pore water can freely flow out of the sediment. This is emulated by stating a constant pressure p_{SWI} along the SWI, so we obtain $p_e \equiv 0$. Note that this constraint was already used to obtain Eq. 3. At the lower boundary, the sediment is either sealed by the core lining (laboratory conditions) or we assume that the flow no longer penetrates deeper layers (natural conditions). Laterally, the sediment is delineated by the core liner, or in situ, we assume a full coverage of the sediment by adjacent *A. marina* domains. Accordingly, at the lower and lateral boundaries, the no-flux condition $\mathbf{v}_d \cdot \mathbf{n} = \nabla p_e \cdot \mathbf{n} = 0$ holds, in which $\mathbf{n}$ is the normal vector pointing from the surface into the sediment. Internally, the feeding pocket constitutes the actual location in which the lugworm pumps burrow water into the sediment. The lugworm itself is modeled as a mechanical pump with a fixed pumping rate Q. Details on the lugworm's pump characteristic can be found in Meysman et al. (in press). Here, it is sufficient to state that the total water flow Q pumped by the lugworm should leave the feeding pocket with surface area A_{fp},

$$Q = \oint_{A_{fp}} \mathbf{v}_d \cdot \mathbf{n} \, dA \tag{5}$$

where $\oint$ denotes the surface integral. The boundary condition along the feeding pocket then determines the vector $\mathbf{v}_d$ in Eq. 5. In theory, there are two possibilities: either the lugworm imposes a constant excess pressure p_e^{fp} along the surface of the feeding pocket, or the discharge of water occurs uniformly through this surface. In practice, however, parameter values for p_e^{fp} are not available in the literature, and only the lugworm's total pumping rate Q is reported. Moreover, the discrimination between an isobaric surface versus uniform discharge conditions turns out to be a rather academic exercise in the case of the lugworm. The radius of the lugworm's feeding pocket is relatively small when scaled to depth of the feeding pocket. Test simulations confirmed that under these conditions, the flow patterns obtained from both boundary conditions become indistinguishable. So rather than an isobaric surface, we assume a uniform discharge, and the magnitude $\|\mathbf{v}_d\|$ of the Darcy velocity vector at the surface of the feeding pocket is calculated as

$$\|\mathbf{v}_d\| = Q / A_{fp} \tag{6}$$

which is the actual boundary condition adopted along the feeding pocket.

Reactive transport model (mass conservation)—The model considers tracer exchange between three separate bodies of water (i.e., the overlying water column, the burrow water, and the interstitial pore water in the sediment). In general, these waterbodies can differ in composition; hence, for a particular tracer, the model needs to respectively determine the concentration in the overlying water column (C^w), the burrow water concentration (C^b), and the concentration in the sediment pore water (C^s). We assume that the overlying water and burrow water are completely mixed. As a consequence, $C^w(t)$ and $C^b(t)$ depend only on time t and not on spatial coordinates. Conversely, the pore-water composition $C^s(r, z, t)$ is described in a spatially explicit fashion over the 2D axisymmetric sediment domain.

Once the velocity field is computed, the velocity $\mathbf{v}$ can be incorporated into the reactive transport equation for the pore-water concentration C^s for a conservative tracer (Bear 1972; Bear and Bachmat 1991; Boudreau 1997)

$$\frac{\partial C^s}{\partial t} + \nabla \cdot (-\mathbf{D} \cdot \nabla C^s + \mathbf{v} C^s) = 0 \tag{7}$$

where $\mathbf{D}$ denotes the hydrodynamic dispersion tensor and $\mathbf{v}$ the pore-water velocity vector. Because the porosity is assumed constant over the sediment domain, porosity terms can be removed from Eq. 7. The hydrodynamic dispersion tensor $\mathbf{D}$ includes the effects of both molecular diffusion and mechanical dispersion and is therefore typically decomposed as $\mathbf{D} = \mathbf{D}^{mol} + \mathbf{D}^{mech}$ (Bear and Bachmat 1991; Oelkers 1996). The tensor for molecular diffusion can be stated as

$$\mathbf{D}^{mol} = (1 - 2 \ln \phi)^{-1} D^{mol} \mathbf{I} \tag{8}$$

where $\mathbf{I}$ denotes the unit tensor, D^{mol} represents the scalar molecular diffusion coefficient, and the factor $(1 - 2 \ln \phi)^{-1}$ represents a correction for tortuosity (Boudreau 1996). The molecular diffusion coefficient D^{mol} for Br^- and NO_3^- are calculated as a function of temperature T and salinity S with use of the relations in Boudreau (1997). The mechanical dispersion tensor $\mathbf{D}^{mech}$ is typically expressed as (Freeze and Cherry 1979; Lichtner 1996)

$$\mathbf{D}^{mech} = D_T \mathbf{I} + \frac{1}{\|\mathbf{v}\|^2} (D_L - D_T) \mathbf{v}\mathbf{v}^T \tag{9}$$

where D_T and D_L are the transversal and longitudinal dispersion coefficients, respectively. The constitutive expression for the latter coefficients are taken from Oelkers (1996)

$$D_T = D^{mol}0.5\{Pe\}^{1.2} \quad (11)$$

$$D_L = D^{mol}0.015\{Pe\}^{1.1} \quad (12)$$

and are valid for Peclet numbers in the range 1–100. The appropriate (grain-scale) Peclet number is calculated as $Pe \equiv d_{50}\|\mathbf{v}\|/D^{mol}$, where d_{50} denotes the median grain size. Velocities, and hence Peclet numbers, are highest at the surface of the feeding pocket and decrease with distance. In our simulations, typical Peclet values ranged in the order of 100 near the injection pocket but dropped rapidly below 1 a couple of centimeters away from the feeding pocket. This indicates that the contribution of mechanical dispersion (Eq. 9) in total hydrodynamic dispersion was only important in a restricted zone around the feeding pocket.

Equation 7 produces the concentration field over the sediment domain, given a proper set of initial and boundary conditions. As initial conditions, we assume a uniform tracer concentration C_0^s in the pore water. At the sediment–water interface, the concentration is set to the concentration $C^w(t)$ of the overlying water column, which can be time dependent in laboratory incubations. In the latter case, $C^w(t)$ results from the water column model (*see* the next section). Laterally, and at the bottom of the domain, the boundary is impenetrable to mass, as it is to flow (i.e., $\nabla C^s \cdot \mathbf{n} \equiv 0$). The burrow water composition is not considered to be influenced by reactive processes within the burrow or by the diffusive transfer across the burrow walls (i.e., $C^b(t) = C^w(t)$. The latter is justifiable because, over the short timescales modeled, only a small diffusive loss occurs via the burrow wall (Table 2). Still, the composition of the water that is actually pumped through the surface of the feeding pocket can deviate from that of the burrow water as a result of the lugworm's metabolism (e.g., when using oxygen as a tracer). In general, we model this metabolic effect as a fractional decrease, $0 < \lambda \leq 1$, and along the feeding pocket, we specify the boundary condition $C^s \equiv \lambda C^b(t)$. For the conservative tracers considered here, $\lambda = 1$.

Water column model (mass conservation)—The water column overlying the sediment is assumed to be well mixed, and its initial tracer concentration is denoted C_0^w. The evolution of the concentration of a conservative tracer is governed by the balance equation

$$V\frac{\partial C^w}{\partial t} = \int_{S_{SWI}} \mathbf{F}\, d\mathbf{S} - QC^w \quad (13)$$

where V is the volume of the overlying water column and Q the pumping rate of the lugworm. The integral term in Eq. 13 accounts for the tracer flux $\mathbf{F}$ coming from the sediment across the surface S_{SWI} of the sediment–water interface. In the general case, this flux $\mathbf{F}$ will depend on time and space and must be calculated from the reactive transport model (Eq. 7).

However, when the incubation period is sufficiently short, one can assume that injection hasn't yet influenced the tracer in the uppermost layer of the sediment and neglect diffusional transfer across the sediment–water interface. In this case, the flux across the sediment–water interface can be approximated as $\int \mathbf{F}d\mathbf{S} \approx QC_0^s$ and Eq. 13 simplifies to

$$V\frac{\partial C^w}{\partial t} = Q(C_0^s - C^w) \quad (14)$$

which has the solution in Eq. 15.

$$C^w(t) = C_0^s + (C_0^w - C_0^s)\exp[-(Q/V)t] \quad (15)$$

Equation 15 predicts an exponential dilution/enrichment signal in the overlying water.

Numerical solutions—In all simulations, Laplace Eq. 4, reactive transport Eq. 7, and water column Eq. 13 were solved numerically with the finite element package FEMLAB version 3.0a (www.comsol.com). Figure 2b shows the unstructured finite element mesh over the sediment domain used in the 2D pocket injection model. The mesh is refined near the feeding pocket to properly resolve the flow in that region. The lower boundary of the model domain must be chosen sufficiently deep to avoid unwanted boundary effects. By taking the domain's lower boundary 10 cm below the depth of the feeding pocket (i.e., $H_s = H_{fp} + 10$, we found that simulation results were virtually the same as for a semi-infinite domain.

Comparison to experimental data

The simulation output from the 2D pocket injection model is compared with data gathered from two separate types of incubation experiments with inert tracers. A first type is referred to as the injection experiment. Here, the injection of Br^- from the overlying water into the sediment as a result of lugworm pumping is evaluated. A second type is referred to as the flushing experiment. Here, the sediment is initially preloaded with a high tracer concentration (NO_3^-) while the overlying water column is initially tracer free. The appearance of tracer in the water column because of *A. marina* bioirrigation is modeled.

Br^- injection experiment—To evaluate the injection of tracer at depth, published pore-water data on Br^- were compared with modeled depth profiles. Details on experimental setup, core sectioning, and analytical methods can be found in Rasmussen et al. (1998). Additional experimental data and measured parameters are reported in Timmermann et al. (2002), in which a one-dimensional (1D) reactive transport model of lugworm irrigation is presented. Because of space limitation, this 1D model is not discussed here. Yet, its output is compared in detail to the 2D pocket injection model presented here in a dedicated paper on 1D/2D/3D models of lugworm bioirrigation (Meysman et al. unpubl. data). In six incubation experiments, dissolved Br^- was used as an inert tracer to study the nonlocal tracer injection into deeper sediment layers by *A. marina* pumping. Polyvinyl chloride tubes were filled with wet sediment (sieved <1 mm) from Roskilde fjord (Denmark). On top, 250 mL of overlying seawater was continuously stirred and aerated. At the start of the experiment, the overlying water was replaced by sea-

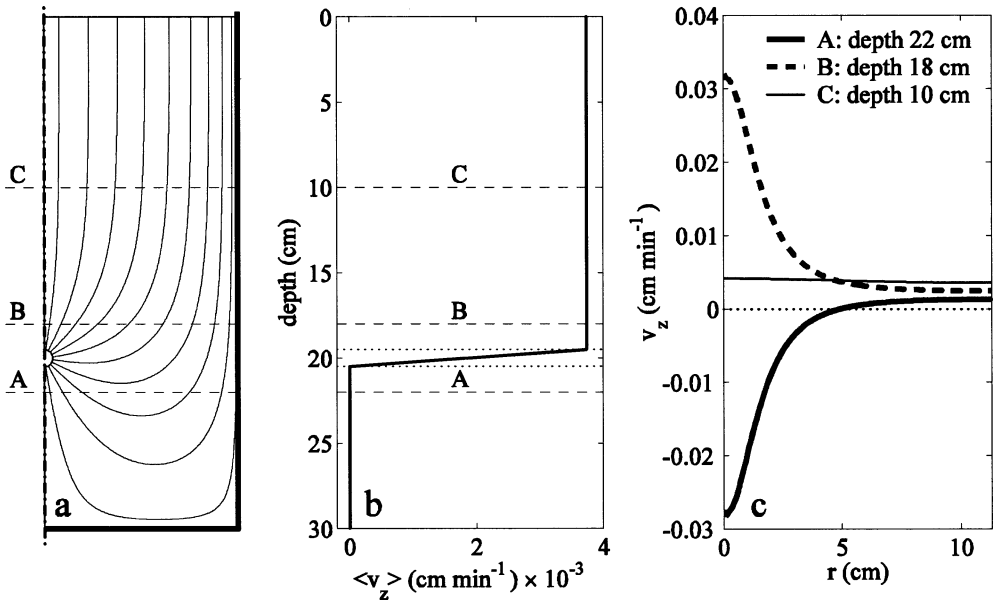

Fig. 3. (a) Flow line pattern simulated by the 2D pocket injection model. Two distinct zones are present: a lower radiation zone, in which flow lines radiate in all directions from the feeding pocket, and an upper percolation zone, in which flow lines are lined up parallel to the vertical. (b) The advective velocity $\langle v_z \rangle$ is obtained by laterally averaging the velocity field resulting from the 2D axisymmetric model. (c) The vertical velocity component v_z as a function of the radial distance at three different depths, A, B and C.

water spiked to about 10 mmol L^{-1} KBr, and a single lugworm (wet weight 0.6–6.2 g) was introduced. After a short incubation period of 1.2–1.9 h at fixed temperature, cores were sectioned and centrifuged, and the Br^- concentration in the filtered pore water was determined.

NO_3^- flushing experiment—To evaluate the exchange between pore water and overlying water, new experiments were performed with NO_3^- as an inert tracer. Nitrate was preferred over bromide because it allowed continuous monitoring via an electrode, rather than discrete sampling over a limited number of time intervals. Lugworms were added to sediment cores that were loaded with a high concentration of NO_3^- in the pore water. Subsequently, the ''flushing'' of the sediment (i.e., the appearance of NO_3^- in the overlying water) was monitored. To this end, clean fine sand (0.03% organic C, median grain size 220 μm) was mixed with NO_3^--amended artificial seawater (30 salinity) before it was transferred into acrylic core liners (25 cm long and 11.2 cm i.d.). Core 1 was filled with this sediment mixture to a height of 8.5 cm, and core 2 was filled to a height of 10 cm. While filling core 2, a 2-mm mesh was inserted horizontally at 5 cm below the sediment–water interface. The mesh acted as a mechanical barrier to prevent *A. marina* from burrowing below this depth. Given the large mesh size, we assumed that the mesh did not influence the advective transport of pore-water constituents. Sediment was left with ~6 cm of aerated overlying water column to stabilize for ~2 h before one *A. marina* was added to each core. *A. marina* specimen were collected from an intertidal flat (in situ salinity ~30) in the Oosterschelde (The Netherlands) and left to acclimatize 1 d before use.

Experiments were initiated by carefully removing the overlying water and replacing it with 300 mL of NO_3^--free artificial seawater. The NO_2^- + NO_3^- concentration in the overlying water was continuously measured with a nitrate biosensor (Unisense NOx biosensor) and recorded with a strip chart recorder. Each experiment was run for approximately 24 h, and the sensor was calibrated immediately before and after each experiment. Experiments were started 12 and 1 h after introduction of *A. marina* in cores 1 and 2, respectively. All experiments were carried out at 15°C, and the overlying water was well aerated at all times. Given the short timescale of the experiment, the high NO_3^- concentration in the pore water (200–600 μmol L^{-1}), the low organic carbon content of the sand, and the use of artificial seawater, microbial activity (nitrification, denitrification) was assumed negligible, so NO_3^- could be considered an inert tracer. Moreover, post hoc mass balance calculations showed conservation of nitrate during the incubation experiment.

Results

Flow line pattern—The flow pattern resulting from the 2D axial symmetric model is shown in Fig. 3a. Basically, this flow line pattern consists of two separate zones: (1) a lower radiation zone, where flow lines radiate from the feeding pocket and diverge in various directions, and (2) an upper percolation zone, where flow lines curve to the sediment–water interface and line up parallel to the vertical. Figure 3b shows the radially averaged velocity $\langle v_z \rangle$. As required by mass conservation, $\langle v_z \rangle$ vanishes below the feeding pocket and is constant above. To illustrate the extent of the radiation

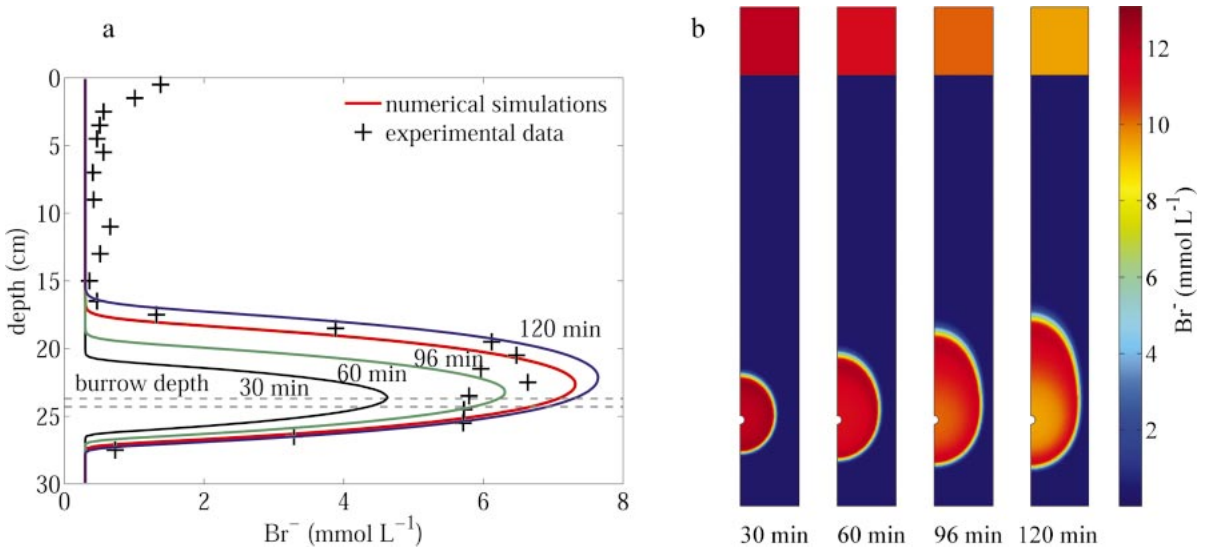

Fig. 4. (a) Dynamical simulation of Br^- injection in the sediment by *Arenicola* pumping employing the 2D pocket injection model. Data (+) correspond to the incubation experiment ''2e'' in Timmermann et al. (2002). Solid lines denote simulated tracer profiles at various incubation times, illustrating the buildup of the tracer plume. The red line represents the simulation for the actual incubation time (96 min). (b) The output of the model, that is, 2D plots of the Br^- concentration at various incubation times. Note the growth of the injected Br^- plume at depth and the simultaneous decrease of the Br^- concentration in the overlying water.

and percolation zones, Fig. 3c plots the vertical velocity component as a function of the radial distance r for the three different horizontal cross sections marked in Fig. 3a (A/B/C). Below the feeding pocket (cross section A) the vertical velocity component v_z changes sign: flow lines head downward (negative v_z) near the core center and head upward (positive v_z) near the sidewalls. The reader should not be misled by the fact that the ''positive'' area under the curve (i.e., the integral for positive v_z) seems smaller than the ''negative'' part (i.e., the integral for negative v_z). When properly accounting for the annular surface $dA = 2\pi r\, dr$, the total flux $\int v_z\, dA$ through cross section A vanishes. Just above the feeding pocket (cross section B) v_z is always positive but varies strongly with radial distance. The highest velocities are near the core center. Finally, at a substantial height above the feeding pocket (cross section C; i.e., when the height above the feeding pocket is larger than the core radius), the dependence of v_z on the radial coordinate becomes weak. This uniform velocity profile is characteristic of the percolation zone.

Br^- injection experiment—We performed dynamical simulations with the 2D pocket injection model to mimic the Br^- accumulation at depth observed in six laboratory core incubations (Rasmussen et al. 1998; Timmermann et al. 2002). First, we describe in detail the modeling procedure for one specific incubation (denoted ''2e'' in Timmermann et al. 2002). Subsequently, we apply the same procedure to the other data. The actual output of the simulations consists of 2D plots of the Br^- concentration at a given incubation time (Fig. 4b). To allow comparison with the 1D data profile resulting from core sectioning, the model output was laterally integrated to produce the average concentration within a given depth layer (Fig. 4a).

Table 3 provides an overview of the 14 parameters that are incorporated in the 2D pocket injection model. Direct measurements were available for 10 parameters (Rasmussen et al. 1998; Timmermann et al. 2002). These include the core setup dimensions (i.e., the inner radius, $R_c = 4.1$ cm; the sediment height, $H_s = 30$ cm; and the height of the overlying water layer, $H_w = 4.7$ cm, corresponding to a volume of 250 mL). The ambient temperature ($T = 15$°C), the salinity of the tracer solution ($S = 15$), and the sediment porosity ($\phi = 0.30$) were equally documented. Furthermore, the incubation time was recorded ($t_f = 96$ min), and the initial concentration in the overlying water was measured (C_0^w mmol L^{-1}). Finally, observations were made on two lugworm characteristics: the location of the lugworm at the end of the incubation (assumed to be depth of the feeding pocket, $H_{fp} = 20$ cm) and the burrow radius ($R_b = 0.3$ cm).

Although no direct measurements were available, the remaining four parameters could be tightly constrained. First, no value for the median grain size d_{50} was reported. Yet, the sediment was characterized as ''very permeable'' (Timmermann et al. 2002); accordingly, we imposed a grain size ($d_{50} = 300$ μm) typifying a medium-coarse sand flat. Effectively, the parameter d_{50} does not greatly influence the simulations because it is only used in the mechanical dispersion relations in Eqs. 11 and 12. The modeled tracer profiles are dominated by advection, with only a moderate influence of dispersion. Second, the initial bromide concentration in the pore water (C_0^s) was not included in the data set but can be directly estimated from its typical concentration of 0.825 mmol L^{-1} in seawater of 33 salinity. Linearly rescaling this value to the ambient salinity of 15 yields $C_0^s = 0.375$ mmol L^{-1}, which nicely matches the baseline concentration in the observed data profile (Fig. 4a). Third, the burrow consumption factor is simply set equal to 1 (i.e., $\lambda \equiv 1$). We adopt the evident assumption that the lugworm's metabolism has no effect on bromide chemistry. Consequently, Br^- concentra-

Table 3. Parameter values used in the simulation of tracer experiments with the axisymmetric 2D model. All parameter values were determined a priori on the basis of experiments and logical constraints, except when values are bracketed. In the latter case, the values between brackets denote the original values, and values outside brackets represent those that were adapted a posteriori to improve fits (see explanation in text). The parameter values in the Br^- column correspond to the simulation output shown in Fig. 4 and, hence, incubation experiment 2e in Timmermann et al. (2002).

		Tracer experiment		
Parameter	Units	Br^-	NO_3 (Core 1)	NO_3 (Core 2)
Core setup				
Core radius (R_c)	cm	4.1	5.6	5.6
Sediment height (H_s)	cm	30	8.5	10
Height overlying water column (H_w)	cm	4.7	3.05	3.05
Experimental conditions				
Temperature (T)	°C	15	15	15
Salinity (S)		15	30	30
Porosity (ϕ)		0.30	0.68	0.65
Median grain size ($\bar{\gamma}$)	μm	300	220	220
Incubation parameters				
Incubation time (t_{final})	min	96	>1,200	>1,500
Initial concentration, overlying water (C_0^w)	mmol L^{-1}	13.1	0	0
Initial concentration, pore water (C_0^s)	mmol L^{-1}	0.37	0.385	0.364
A. marina parameters				
Depth, feeding pocket (H_{fp})	cm	(20)24	7	5
Radius, feeding pocket (R_{fp})	cm	0.3	0.25	0.25
Burrow depletion factor (λ)		1	1	1
Pumping rate (Q)	cm^3 min^{-1}	(0.76)0.68	1.3	0.3

tion in the water injected across the wall of the feeding pocket always equals that in the overlying water (i.e., $C^b(t) = C^w(t)$).

Given the above, the model still contains one unconstrained parameter (i.e., the pumping rate Q). A direct measurement of this parameter is difficult and laborious. However, the bromide concentration in the overlying water at the end of the incubation was reported (i.e., $C_f^w = 9.8$ mmol L^{-1}; Timmermann et al. 2002). On this basis, Q can be indirectly assessed with the use of some simple mass balance considerations. To this end, we can follow two approaches that are based on the inventory change of the tracer in the overlying water and the pore water, respectively. The tracer's inventory change in the overlying water is calculated as $\Delta I^w = V(C_0^w - C_f^w)$, which provides a value of $\Delta I^w = 825$ μmol. By suitably rearranging Eq. 15, one can estimate the pumping rate

$$Q = -\frac{V}{t_f}\ln\left[1 - \frac{\Delta I^w}{V(C_0^w - C_0^s)}\right] \tag{16}$$

yielding a first estimate of $Q = 0.78$ cm^3 min^{-1} for the pumping rate. Alternatively, we can calculate the inventory increase of the bromide in the pore water by integration of the depth profile as

$$\Delta I^s = \phi A \int_0^{H_s} [C^s(z, t_f) - C_0^s]\, dz \tag{17}$$

providing the value $\Delta I^s = 806$ μmol. Mass conservation requires that the inventory changes in both overlying water and pore water should match (i.e., $\Delta I^w = \Delta I^s$), and our estimates closely match this theoretical prediction. When substituting $\Delta I^s = 806$ μmol rather than $\Delta I^w = 825$ μmol in Eq. 16, we obtain the slightly different pumping rate of $Q = 0.76$ cm^3 min^{-1}. Both estimates of Q are in close agreement, and in the simulations, we implemented $Q = 0.78$ cm^3 min^{-1}.

A principal achievement of the above parameter analysis is that all 14 model parameters could be constrained a priori. Figure 4 shows the model output at consecutive times spanning a total incubation period of 120 min. To fit the experimental data, only two of the initial parameter values needed adjustment (Table 3). The feeding pocket depth was adjusted to 24 cm, which is somewhat deeper than the observed 20 cm where the worm was located at the end of the experiment. This can be explained by a small change in the lugworm's position before or during core sectioning (Timmermann et al. 2002). Second, the pumping rate was slightly lowered to a value of $Q = 0.68$ cm^3 min^{-1}. This adjustment is not unexpected because our approximation from Eq. 16 tends to overestimate the pumping rate. This calculation does not account for diffusional transfer across the sediment–water interface and burrow walls; consequently, any changes in the inventory of the overlying water and the sediment pore water is solely attributed to lugworm pumping. Therefore, the downward adjustment of the pumping rate seems justifiable.

When implementing the adjusted parameter set, the computed tracer concentration closely matches the experimental data profile after 96 min of pumping (i.e., the actual length

of the experimental incubation period). The tracer profiles show five conspicuous aspects. (1) A subsurface peak of Br^- builds up at the feeding depth of the lugworm. With time, this peak broadens and its maximum increases. (2) This peak broadening is asymmetric, with the tracer penetrating the sediment faster above than below the feeding pocket. This can be explained in terms of the average pore-water flow (Fig. 3b), which vanishes under the feeding depth but pushes the tracer upward above the feeding depth. This leads to a faster expansion of the tracer plume above the feeding pocket than below. (3) The peak of the tracer concentration does not occur exactly at the center of the feeding pocket, but slightly higher up in the sediment core. This peak shift emerges in two ways. The first—obvious—reason is the reduction of the tracer concentration in the overlying water with time. The pumping activity of the lugworm expels pore water low in bromide across the sediment–water interface and, hence, dilutes the overlying water. However, even in the case in which the tracer concentration in the overlying water is kept constant, the peak tracer concentration maximum can be offset (simulations not shown). The interplay of radiation and percolation generates a 3D tracer plume that has an ellipsoidal shape (*see Fig. 4*). The depth at which this ellipsoidal tracer plume is at its broadest does not need to coincide with the depth of the injection pocket. (4) The data profile has a baseline concentration around $C_0^s = 0.4$ mmol L^{-1}, which extends above and below the subsurface peak. This matches the background concentration of bromide in the pore water as calculated above. Accordingly, this baseline does not result from diffusion across the burrow wall. On the timescale of the incubation (96 min), bromide can only penetrate ~4 mm from the burrow by diffusive transport, and the corresponding effect on the layer-averaged concentration is negligible. (5) The data show considerable ''intrusion'' of the tracer below the sediment–water interface, penetrating to about 3 cm depth in 96 min. This feature is however not reproduced in the model simulations. Molecular diffusion cannot explain such deep penetration of tracer (even in the absence of upward advection). The timescale of the incubation (96 min) is simply too small to allow diffusive transport 3 cm downward. The observed anomalous tracer intrusion could be an artifact of core sectioning: when slicing the uneven sediment–water interface, tracer-rich overlying water could be included in the top slice. Alternatively, the intrusion might also be the result of the intensive stirring of the overlying water during the incubations (Khalili et al. 1999). This cross-surface exchange induced by stirring provides another justification for the downward adjustment of the pumping rate Q from 0.78 to 0.68 cm^3 min^{-1}.

Figure 5 shows data and simulated profiles for the five core incubations in addition to the one depicted in Fig. 4. The same modeling procedure was followed as detailed earlier: 2D pocket injection model, a priori fixation of parameters, and estimation of the pumping rate Q via Eq. 16. The parameter values are summarized in Table 4. Figure 5 shows two different types of simulated concentration profiles in addition to the data points. The dashed lines represent simulations in which the feeding pocket has the standard shape (i.e., a sphere of the same diameter as the burrow). A good fit between the data and the concentration profiles was obtained in two profiles (Fig. 5d,e). For the other four profiles, the base of the tracer plume was wider and its peak concentration lower than predicted by the model. To better fit the data, we altered the shape of the feeding pocket and replaced its default spherical shape with an elliptic one, with the long axis oriented upward. This vertical extension of the feeding pocket means that burrow water is now injected over a larger depth zone. In terms of model formulation, this implies the introduction of one additional parameter: the elliptic feeding pocket is now described by a minor radius R_{fp}^{min} and a major radius R_{fp}^{max}. We fixed the minor radius to the burrow radius (i.e., $R_{fp}^{min} = R_b$), whereas the major radius was used as the fitting parameter. The proposed modification of the feeding pocket can be justified for several reasons. First, we assumed by default that the feeding pocket has the same radius as the burrow. This rather naive assumption most probably underestimates the size of the lugworm's feeding pocket under natural conditions. Second, the experimental cores have a rather small diameter, which might prevent the lugworm from building a typical horizontal gallery. Instead, the gallery could be curved upward, creating a vertically extended injection zone. Third, biological behavior (feeding, burrowing) characteristically induces variability in ecological experiments. In our case, the lugworm might reposition during incubation experiments. As a consequence, the injection depth could shift over the course of an incubation and extend the injection zone in the vertical.

Overall, the Br^- injection experiment reveals a substantial agreement between the data of Rasmussen et al. (1998) and the simulation output of the 2D pocket injection model (especially given the strong data constraints on the parameters). The introduction of one additional parameter (extending the parameter from 14 to 15) to account for biological variability does not weaken the model's mechanistic character in our view. The solid lines in Fig. 5 represent simulations in which the feeding pocket has the elongated elliptical shape. Table 4 documents the values for the major radius R_{fp}^{max} that produce the best fits. The estimated range for the feeding pocket elongation of parameter values showed that moderate variation and parameter values might reflect actual repositioning distances and inherent variability in shape of the feeding pocket.

NO_3^- flushing experiment—To further test the model, the NO_3^- flushing experiment focuses on concentration changes in the overlying water rather than the pore water. Figure 6a shows the evolution of the nitrate concentration in the overlying water for two separate experiments. Between experiments, two parameters were varied that were thought of as critical: the feeding depth and the pumping rate. In core 1, a relatively large lugworm was introduced (expected to show a relatively large pumping rate), and no attempt was made to control its feeding depth. After introduction, visual inspection revealed that the lugworm established a burrow close to the bottom of the core. In core 2, a smaller individual was introduced (with a smaller pumping rate) that was prohibited from burrowing deeper than 5 cm by placing a mesh at that depth. It was observed that the lugworm burrowed until it encountered the obstructing mesh.

The tracer concentration data in the water overlying core

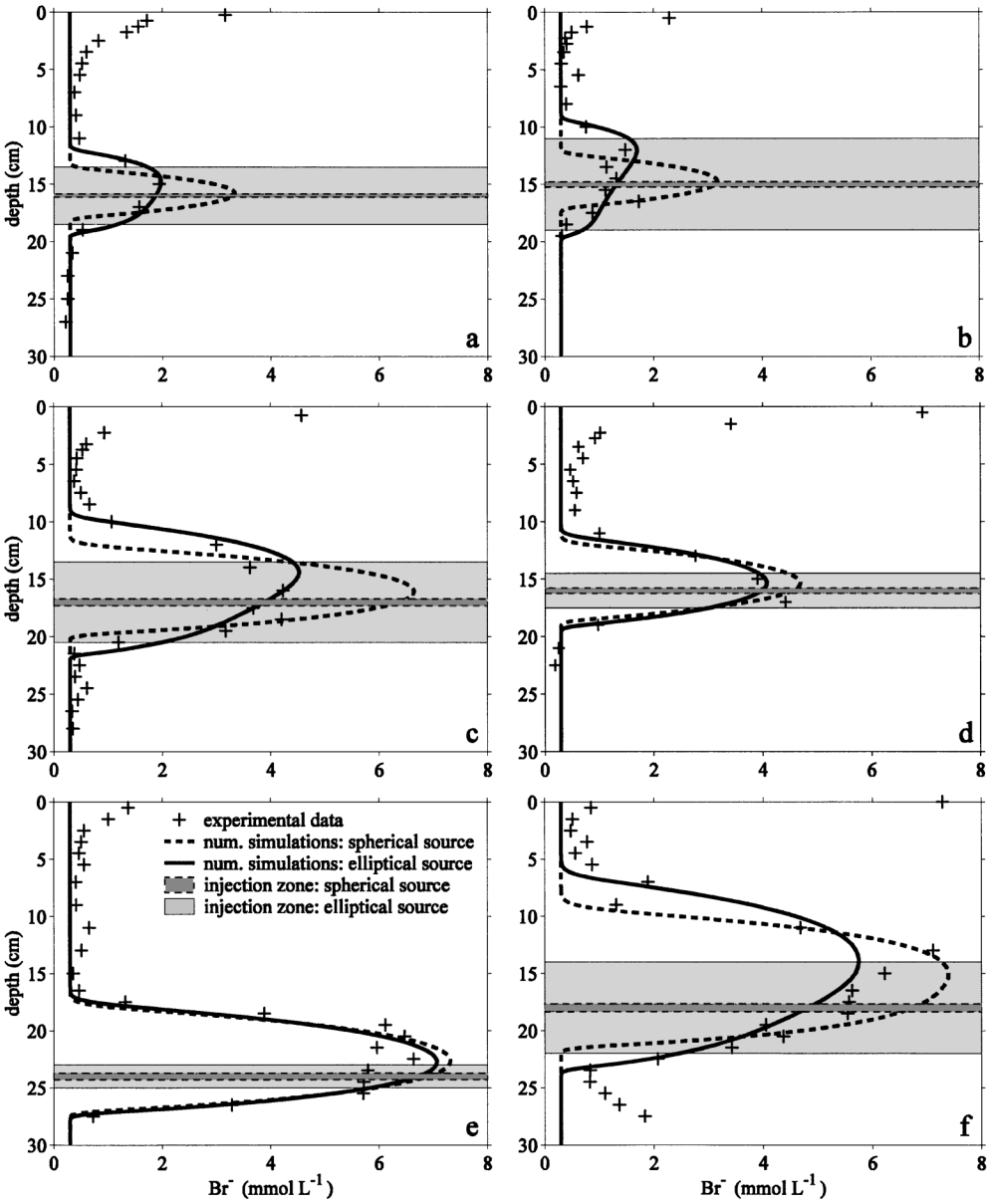

Fig. 5. Comparison of data and simulations for all Br^- injection experiments reported in Timmermann et al. (2002). Plus symbols represent Br^- pore-water data from core slicing. Dashed lines denote simulations with the 2D axisymmetric model without an extra fitting parameter. The radius of the spherical feeding pocket (dark gray zone) is the same as the burrow radius. Solid lines denote the best fit when including one additional fitting parameter. The feeding pocket is vertically elongated, resulting in elliptical shape with fixed minor radius and optimized major radius. The light gray zone illustrates this vertical extension of the feeding pocket.

2 (small worm) show a gradual and smooth (i.e., monotonically increasing) evolution, indicating a relatively slow release of nitrate from the sediment. At the end of the incubation (after 1,500 min), the concentration is still rising, indicating that the system has not yet reached a steady state. In contrast, the tracer evolution in core 1 (big worm) is markedly different. The release of NO_3^- is much faster and reaches a steady state after about 800 min. In the steady-state situation, pore water and overlying water are completely mixed; thus, they attain the same NO_3^- concentration (252 μmol L^{-1}). The most conspicuous feature in the core 1 data is the nonmonotonic increase of the NO_3^- concentration in the overlying water. On the way to steady state, at about 300 min, the NO_3^- concentration overshoots the final steady-state value. Although the overshoot is small, it is not an artifact because its magnitude is well above the analytical error of the nitrate electrode. Moreover, the appearance of a concentration maximum is plausible from a physical point of view. The lugworm pumping expels a volume of high NO_3^- pore water, which temporarily causes the concentration in the

Table 4. Parameter values employed in simulation of the Br^- injection experiments of Rasmussen et al. (1998). The corresponding simulation output is depicted in Fig. 5. Markers a–f correspond to the data profiles as reported in Timmermann et al. (2002, fig. 2). The parameter values for the incubation time t_{final}, the minor radius of the feeding pocket $R_{fp}^{min} = R_b$, and the depth of feeding pocket H_{fp} are based on measurements as reported in Timmermann et al. (2002, table 1). The pumping rate Q is estimated from the final Br^- inventory as discussed in the text. The major radius of the feeding pocket is used as a fitting parameter to improve model fits (*see* text and Fig. 5).

Incubation experiment	Units	Marker					
		a	b	c	d	e	f
Incubation time (t_{final})	min	72	78	75.6	84	96	114
Minor radius, feeding pocket (R_{fp}^{min})	cm	0.15	0.25	0.30	0.25	0.30	0.35
Depth, feeding pocket (H_{fp})	cm	16.0	15.0	17.0	16.0	24.0	18.0
Pumping rate (Q)	$cm^3\ min^{-1}$	0.175	0.192	0.683	0.425	0.687	1.017
Major radius, feeding pocket (R_{fp}^{max})	cm	2.5	4.0	3.5	1.5	1.0	4.0

overlying water to exceed the final equilibrium value. The latter equilibrium concentration is attained when pore water and overlying water are fully mixed with one another. Note that the overshoot was revealed by continuous electrode monitoring and would have been overlooked if a coarser, discrete sampling procedure had been used.

To test our interpretation of the overshoot mechanism, we simulated the incubations in cores 1 and 2 with the 2D pocket injection model. Effectively, we first performed the experiment with core 1, performed the associated model simulation, and predicted where the mesh should be placed to avoid the overshoot mechanism. We subsequently performed the experiment with core 2 as a test. In both simulations, we adopted the same attitude toward parameters as in the Br^- injection experiment, constraining parameters as much by measurements as possible. Effectively, 13 parameter values could be fixed a priori (Table 3), with the pumping rate Q remaining as a single fitting parameter. The simulated evolution of the NO_3^- concentration in the overlying water is depicted by the solid lines in Fig. 6a. The pumping rates in core 1 and core 2 were estimated as 1.3 and 0.3 $cm^3\ min^{-1}$, respectively. These values reflect the difference in size of the organisms that were used in the incubations. The general shape of the data profiles and, in particular, the overshoot of the tracer concentration in core 1 are well reproduced.

The overshoot peak is a characteristic trait of the data and, hence, a suitable feature to validate the proposed bioirrigation model. Given the different results from core 1 and core 2, our incubations indicate that the presence and magnitude of the overshoot peak is controlled by the geometric parameters of the system and, in particular, by the depth of the lugworm's feeding pocket. When the feeding pocket depth becomes shallower, a smaller volume of tracer-free water can be stored. At the same time, the removal of nitrate-rich pore water from the sediment is more gradual because of retardation of tracer in the deeper sediment layers below the feeding pocket (Fig. 6b, right panel). Both of these trends oppose the occurrence of an overshoot. To illustrate this, we plotted the 2D concentration patterns in Fig. 6b that correspond to the maximal concentrations in the overlying water of core 1

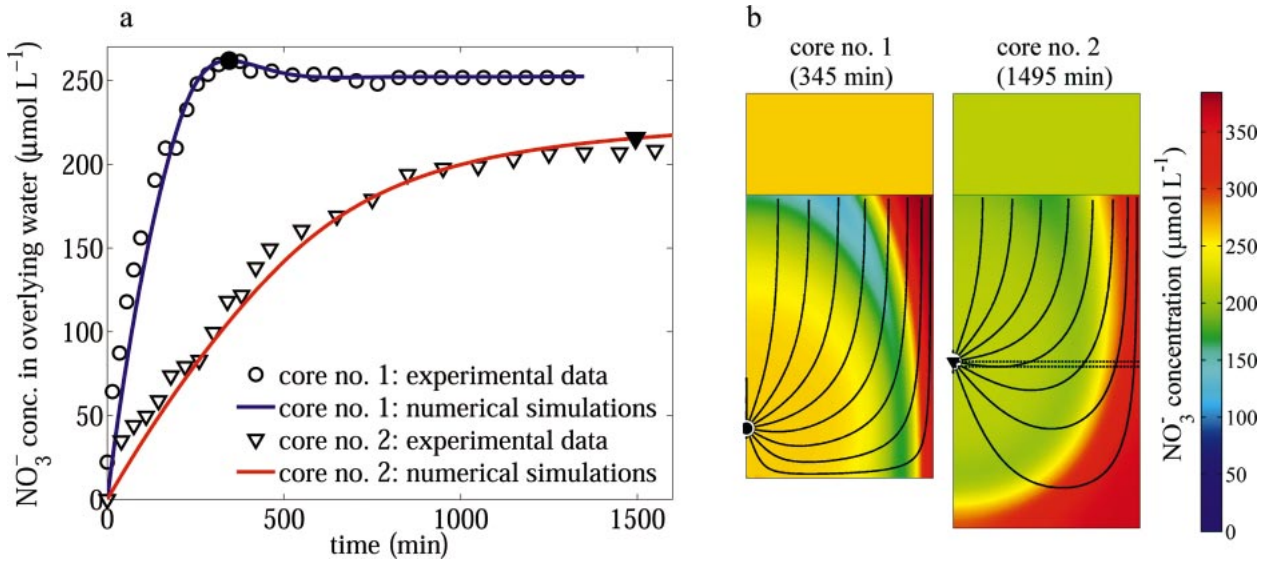

Fig. 6. Dynamical simulation of NO_3^- flushing experiment. (a) Evolution of the tracer concentration in the overlying water for two separate cores (C1 and C2). Data markers show only a selection of the continuous electrode recordings. (b) Tracer concentration plots at a specific point in time indicated by the filled symbols in panel a. Computed flow lines are shown as solid lines. The location of the mesh in core 2 is indicated by the dashed lines.

(350 min, solid circle) and core 2 (1,500 min, solid triangle). The core 1 plot shows that a considerable volume of low-nitrate pore water is present inside the sediment core. In contrast, the core 2 plot shows a rather large zone (dead corner) in which the tracer has not been removed. Additional simulations with varying H_{fp} (result not shown) confirmed that the presence of an overshoot critically depends on the feeding pocket location, corroborating the above explanation of the overshoot mechanism. Also, these simulations emphasize that advective flows beneath the feeding depth are crucial in simulating reactive transport.

Discussion

Both in muddy and sandy environments, bioirrigation is driven by the same biological cause: burrow flushing. Macrofauna circulate overlying water through their burrows to ensure oxygen supply, for metabolite removal, and because of filter feeding. Similarly, both in permeable and impermeable sediments, this burrow flushing has two strong geochemical consequences: enhanced solute transport within the pore water and an increased exchange across the sediment–water interface. However, the actual physical connection between burrow flushing and increased solute transport is very different in muddy sediments compared with sandy environments. In recent reviews on bioirrigation modeling (e.g., Aller 2001), this dependence of the bioirrigation mechanism on sediment permeability has only been given sparse attention.

Bioirrigation mechanisms: Muds versus sands—In discussions of bioirrigation, the terms irrigation and ventilation are often used interchangeably (Boudreau 1997; Aller 2001). Here we advocate a sharpening of this terminology because the process of bioirrigation involves two separate phenomena at two different locations. In the burrow, water flow is induced by the organism, and this ''hydrodynamic'' process we refer to as *burrow ventilation.* Subsequently, this burrow flow forms the driving force for the enhanced transport of solutes in the pore water surrounding the burrow, and this ''geochemical'' process we refer to as *pore-water irrigation.* We propose this terminology to clearly separate the cause (burrow flushing) from the consequence (enhanced pore-water transport). This separation is necessary because the link between burrow ventilation (the cause) and pore-water irrigation (the consequence) strongly depends on the permeability of the sediment. To this end, we propose a conceptual scheme that distinguishes two end-member situations (Fig. 1): a diffusion-dominated mechanism in muddy environments and a purely advective mechanism in sandy sediments.

In muddy sediments, the burrow flows generated by macrofauna will not penetrate the sediment because of high hydromechanical dampening. Molecular diffusion constitutes the physical process that drives solute exchange across the burrow wall. To achieve circulation, a burrow network must have two or more open connections to the SWI, ensuring a continuous conduit. The U-shaped burrow (Fig. 1a) is the archetypal example of such burrow architecture. In sandy sediments, the burrow flows generated by macrofauna can penetrate the surrounding sediment because of the high permeability (Fig. 1b). Accordingly, organisms can actively pump water across the burrow wall when ventilating their burrow. Advection is now the physical process responsible for the exchange of substances across the burrow wall. In terms of burrow architecture, tubes are allowed to have a dead end within the sediment. The lugworm's J-shaped burrow forms a prototypical example of this burrow architecture. After passing the organism, the burrow water percolates through the sediment up to the SWI.

Bioirrigation models: Tube irrigation versus pocket injection—This difference between diffusive and advective bioirrigation mechanisms is also reflected in the types of bioirrigation models that can be constructed. A comparison of the tube irrigation model developed by Aller (1980) with the pocket injection model presented here provides insight into the general structure of a bioirrigation model. Both tube irrigation and pocket injection models have a similar structure, which is essentially based on two steps: (1) the selection of a proper set of model equations that describe the physical connection between burrow flushing and pore-water transport and (2) the selection of a simplified sediment geometry in which these model equations are implemented.

These two modeling choices are common to any mechanistic bioirrigation model and involve specific challenges. The first step, the selection of the relevant model equations, is rather straightforward. In the tube irrigation model, the basic assumption is that bioirrigation is caused by diffusive exchange between the burrow water and the interstitial pore water. Accordingly, the physical transport mechanism is molecular diffusion; hence, the central model equation is given by Fick's Law of diffusion. In contrast, in the pocket injection model, the fundamental assumption is that advection is the dominant transport mode of interstitial solutes. Accordingly, pore-water flow is selected as the dominant physical transport mechanism; hence, Darcy's Law is used to model the flow pattern in combination with a reactive transport model. The difficult step in the development of a mechanistic bioirrigation model is the second step: the selection of the appropriate model geometry. Bioirrigated sediments include intricate 3D structures featuring complex burrow shapes that can be interconnected or not. A crucial question is then how to idealize this sediment complexity without losing some essential features that govern bioirrigation. Mathematically, this idealization procedure involves the selection of a proper geometry for the model domain and an adequate choice of boundary conditions over this geometry.

Remarkably, the problem of geometric idealization is very similar in both diffusion-dominated and advection-dominated systems, as shown by the configuration of the tube irrigation and the pocket injection models. First, both models implement a strong abstraction of natural sediments that are idealized as a collection of identical ''average territories'' inhabited by a single organism. Similarly, the average territory is modeled as a cylindrical domain, in which the radius is determined by the density of the organism. Second, both models propose a drastic simplification of the burrow structure, so that model domain becomes axisymmetric. In the tube irrigation model, the average burrow is a straight cylindrical burrow structure (Fig. 1a). In the pocket injection

model (Fig. 1b), the actual geometry of the burrow is neglected but for the location of an injection pocket. Third, both models propose a strongly simplified picture of the pumping behavior of the macrofauna. In the tube irrigation model, the organisms are simply considered ''mixing devices'' that mix the burrow water with overlying water so that the burrow water is kept at the composition of the overlying water column. In the pocket injection model, the organisms are considered ''pumping devices'' that pump overlying water through the burrow to the feeding pocket and into the surrounding sediment.

Hybrid bioirrigation models—The distinction between the diffusive and advective end-member mechanisms of bioirrigation is certainly attractive from a conceptual viewpoint. Moreover, when confronted with experimental data, the corresponding tube irrigation and pocket injection models are capable of generating realistic output, despite the strong idealizations underlying these models (*see* Aller 1980 for the tube-irrigation model; this study for the pocket injection model). Note however that these model simulations typically apply to controlled laboratory incubations that use conservative tracers. Such incubation experiments are subject to the usual range of idealizations (homogenized sediment, monoculture of a single species, etc.). With respect to natural sediments and reactive constituents, one might expect the situation to be less clear-cut. The bioirrigation mode induced by a certain organism might well be a superposition of diffusive and advective mechanisms. One such situation seems to occur with a highly reactive tracer in sandy sediments such as oxygen. Because consumption within the sediment is high, the oxygen penetration depth from the burrow wall is small, and steep gradients will generate high diffusive fluxes to the sediment. Accordingly, in this situation, both the contributions from advective and diffusive bioirrigation mechanisms must be assessed, and the corresponding bioirrigation model could become a hybrid description.

Lugworm bioirrigation—A. marina is studied here as the prime example of a bioirrigating organism in sandy sediments. The advective flows generated by the flushing of the lugworm's J-shaped burrow form the dominant mode of solute transport in the pore water. So from a quantitative perspective, it is vital to have an accurate description of the pore-water flow induced by lugworm pumping. In theory, this flow pattern can be modeled with the standard description for flow in porous media: Darcy's Law. However, the crucial step in the development of such a flow model is the specification of the geometry of the model domain and, in particular, the idealization of the burrow structure. The 2D pocket injection proposed here greatly simplifies the geometric complexity of the lugworm burrow. The burrow structure is almost completely disregarded, retaining only the feeding pocket as the actual location where burrow water is injected into the sediment. To test this idealization, our model simulations were confronted with data obtained from laboratory incubations with inert tracers. Special care was taken to keep the modeling approach as mechanistic as possible, constraining parameter values a priori on the basis of measurements and refraining from the introduction of parameter fitting. Overall, we obtained an excellent agreement between data and model output, and we were able to reproduce specific system responses (e.g., an overshoot of the tracer concentration in the water column). These results indicate that the flow model underlying the 2D pocket injection model includes an accurate simplification of the flow pattern induced by *A. marina* under laboratory conditions. The most striking feature of this flow pattern is that it consists of two separate zones: a radiation zone around the injection pocket and a percolation zone where flow lines align in parallel, consistent with the flow patterns of 3D flow simulations (Meysman et al. in press).

Evident questions that follow from this are: (1) to what extent does the pocket injection model capture the dynamics of bioirrigation in heterogeneous natural environments, and (2) if and how can it be used to quantify the effects of burrow ventilation by other benthic organisms. Because of the specific geometry tied to the lugworm's burrow, it is unrealistic that the pocket injection model presented here can be applied to other organisms without modification. However, the modeling approach presented here *is* directly transferable. Important features in this regard are (1) the combination of flow (Darcy's Law) and reactive transport modeling and (2) the strong idealization of the burrow geometry to localized injection zones. This way, the present modeling approach can contribute to a better quantitative and conceptual understanding of bioirrigation in permeable sediments.

References

ALLER, R. C. 1980. Quantifying solute distributions in the bioturbated zone of marine-sediments by defining an average microenvironment. Geochim. Cosmochim. Acta **44:** 1955–1965.

———. 2001. Transport and reactions in the bioirrigated zone, p. 269–301. *In* B. P. Boudreau and B. B. Jorgensen [eds.], The benthic boundary layer. Oxford Univ. Press.

———, AND J. Y. ALLER. 1998. The effect of biogenic irrigation intensity and solute exchange on diagenetic reaction rates in marine sediments. J. Mar. Res. **56:** 905–936.

ANDERSON, J. G., AND P. S. MEADOWS. 1978. Microenvironments in marine sediments. Proc. R. Soc. Edinburgh Sect. B **76:** 1–16.

ARCHER, D., AND A. DEVOL. 1992. Benthic oxygen fluxes on the Washington shelf and slope—a comparison of in situ microelectrode and chamber flux measurements. Limnol. Oceanogr. **37:** 614–629.

BAUMFALK, Y. A. 1979. On the pumping activity of *Arenicola marina.* Neth. J. Sea Res. **13:** 422–427.

BEAR, J. 1972. Dynamics of fluids in porous media. American Elsevier.

———, AND Y. BACHMAT. 1991. Introduction to modeling of transport phenomena in porous media. Kluwer.

BENOIT, J. M., T. TORGERSEN, AND J. ODONNELL. 1991. An advection diffusion-model for Rn-222 transport in near-shore sediments inhabited by sedentary polychaetes. **105:** 463–473.

BERG, P., S. RYSGAARD, P. FUNCH, AND M. K. SEJR. 2001. Effects of bioturbation on solutes and solids in marine sediments. Aquat. Microb. Ecol. **26:** 81–94.

BERNER, R. A. 1980. Early diagenesis: A theoretical approach. Princeton Univ. Press.

BOUDREAU, B. P. 1996. The diffusive tortuosity of fine-grained unlithified sediments. Geochim. Cosmochim. Acta **60:** 3139–3142.

———. 1997. Diagenetic models and their implementation. Springer.

———, AND R. L. MARINELLI. 1994. A modeling study of discontinuous biological irrigation. J. Mar. Res. **52:** 947–968.

CHRISTENSEN, J. P., A. H. DEVOL, AND W. M. SMETHIE. 1984. Biological enhancement of solute exchange between sediments and bottom water on the Washington shelf. Cont. Shelf Res. **3:** 9–23.

CRANK, J. 1975. The mathematics of diffusion. Oxford Univ. Press.

DAVIS, R. B. 1974. Tubificids alter profiles of redox potential and pH in profundal lake sediments. Limnol. Oceanogr. **19:** 342–346.

EMERSON, S., R. JAHNKE, AND D. HEGGIE. 1984. Sediment–water exchange in shallow-water estuarine sediments. J. Mar. Res. **42:** 709–730.

FOSTER-SMITH, R. L. 1978. An analysis of water flow in tube-living animals. J. Exp. Mar. Biol. Ecol. **34:** 73–95.

FREEZE, R. A., AND J. A. CHERRY. 1979. Groundwater. Prentice Hall.

FURUKAWA, Y., S. J. BENTLEY, AND D. L. LAVOIE. 2001. Bioirrigation modeling in experimental benthic mesocosms. J. Mar. Res. **59:** 417–452.

GUST, G., AND J. T. HARISSON. 1981. Biological pumps at the sediment–water interface: Mechanistic evaluation of the alpheid schrimp *Alpheus mackayi* and its irrigation pattern. Mar. Biol. **64:** 71–78.

HAMMOND, D. E., H. J. SIMPSON, AND G. MATHIEU. 1975. Methane and radon-222 as tracers for mechanisms of exchange across the sediment–water interface in the Hudson river estuary, p. 119–132. *In* T. M. Church [ed.], Marine chemistry in the coastal environment. American Chemical Society.

HUETTEL, M. 1990. Influence of the lugworm *Arenicola marina* on porewater nutrient profiles of sand flat sediments. Mar. Ecol. Prog. Ser. **62:** 241–248.

———, AND I. T. WEBSTER. 2001. Porewater flow in permeable sediments, p. 144–179. *In* B. P. Boudreau and B. B. Jorgensen [eds.], The benthic boundary layer. Oxford Univ. Press.

HYLLEBERG, J. 1975. Selective feeding by *Abarenicola pacifica* with notes on *Abarenicola vagabunda* and a concept of gardening in lugworms. Ophelia **14:** 113–137.

JONES, S. E., AND C. F. JAGO. 1993. In situ assessment of modification of sediment properties by burrowing invertebrates. Mar. Biol. **115:** 133–142.

KHALILI, A., A. J. BASU, U. PIETRZYK, AND M. RAFFEL. 1999. An experimental study of recirculating flow through fluid–sediment interfaces. J. Fluid Mech. **383:** 229–247.

KORETSKY, C. M., C. MEILE, AND P. VAN CAPPELLEN. 2002. Quantifying bioirrigation using ecological parameters: A stochastic approach. Geochem. Trans. **3:** 17–30.

KRISTENSEN, E. 2001. Impact of polychaetes (*Nereis* spp. and *Arenicola marina*) on carbon biogeochemistry in coastal marine sediments. Geochem. Trans. **2:** 92–103.

KRUGER, F. 1971. Bau und leben des wattwurmes *Arenicola marina*. Helgol. Meeresunters. **22:** 149–200.

LICHTNER, P. C. 1996. Continuum formulation of multicomponent–multiphase reactive transport, p. 1–82. *In* P. C. Lichtner, C. C. Steefel, and E. H. Oelkers [eds.], Reactive transport in porous media. The Mineralogical Society of America.

MARINELLI, R. L., C. R. LOVELL, S. G. WAKEHAM, D. B. RINGELBERG, AND D. C. WHITE. 2002. Experimental investigation of the control of bacterial community composition in macrofaunal burrows. Mar. Ecol. Prog. Ser. **235:** 1–13.

MCCAFFREY, R. J., AND OTHERS. 1980. The relation between pore water chemistry and benthic fluxes of nutrients and manganese in Narragansett Bay. Limnol. Oceanogr. **25:** 31–44.

MEILE, C., C. M. KORETSKY, AND P. VAN CAPPELLEN. 2001. Quantifying bioirrigation in aquatic sediments: An inverse modeling approach. Limnol. Oceanogr. **46:** 164–177.

———, AND P. VAN CAPPELLEN. 2003. Global estimates of enhanced solute transport in marine sediments. Limnol. Oceanogr. **48:** 777–786.

MEYSMAN, F. J. R., O. S. GALAKTIONOV, AND J. J. MIDDELBURG. In press. Sediment irrigation patterns induced by *Arenicola marina* burrow ventilation. Mar. Ecol. Prog. Ser.

OELKERS, E. H. 1996. Physical and chemical properties of rocks and fluids for chemical mass transport calculations, p. 131–191. *In* P. C. Lichtner, C. C. Steefel, and E. H. Oelkers [eds.], Reactive transport in porous media. The Mineralogical Society of America.

RASMUSSEN, A. D., G. T. BANTA, AND O. ANDERSEN. 1998. Effects of bioturbation by the lugworm *Arenicola marina* on cadmium uptake and distribution in sandy sediments. Mar. Ecol. Prog. Ser. **164:** 179–188.

REICHARDT, W. 1988. Impact of bioturbation by *Arenicola marina* on microbiological parameters in intertidal sediments. Mar. Ecol. Prog. Ser. **44:** 149–158.

REISE, K. 2002. Sediment mediated species interactions in coastal waters. J. Sea Res. **48:** 127–141.

RHOADS, D. C. 1974. Organism–sediment relations on the muddy sea floor. Oceanogr. Mar. Biol. **12:** 263–300.

RIISGÅRD, H. U., AND G. T. BANTA. 1998. Irrigation and deposit feeding by the lugworm *Arenicola marina*, characteristics and secondary effects on the environment. A review of current knowledge. Vie Milieu **48:** 243–257.

———, I. BERNTSEN, AND B. TARP. 1996. The lugworm (*Arenicola marina*) pump: Characteristics, modelling and energy cost. Mar. Ecol. Prog. Ser. **138:** 149–156.

ROCHA, C., S. FORSTER, E. KONING, AND E. EPPINK. 2005. High-resolution permeability determination and two-dimensional porewater flow in sandy sediment. Limnol. Oceanogr. Methods **3:** 10–23.

TIMMERMANN, K., J. H. CHRISTENSEN, AND G. T. BANTA. 2002. Modeling of advective solute transport in sandy sediments inhabited by the lugworm *Arenicola marina*. J. Mar. Res. **60:** 151–169.

VANDERBORGHT, J. P., R. WOLLAST, AND G. BILLEN. 1977. Kinetic-models of diagenesis in disturbed sediments. 1. Mass-transfer properties and silica diagenesis. Limnol. Oceanogr. **22:** 787–793.

WEBB, A. P., AND B. D. EYRE. 2004. Effect of natural populations of burrowing Thalassinidean shrimp on sediment irrigation, benthic metabolism, nutrient fluxes and denitrification. Mar. Ecol. Prog. Ser. **268:** 205–220.

WELLS, G. P. 1945. The mode of life of *Arenicola marina* (L.). J. Mar. Biol. Assoc. U.K. **26:** 170–207.

———. 1949. The behaviour of *Arenicola marina* (L.) in sand, and the role of spontaneous activity cycles. J. Mar. Biol. Assoc. U.K. **28:** 465–478.

WENZHÖFER, F., AND R. N. GLUD. 2004. Small-scale spatial and temporal variability in coastal O_2 dynamics: Effects of fauna activity. Limnol. Oceanogr. **49:** 1471–1481.

Received: 5 November 2004
Amended: 18 August 2005
Accepted: 22 August 2005